minerals

MDPI

Article

Fabrication of Single-Crystalline Calcite Needle-Like Particles Using the Aragonite–Calcite Phase Transition

Yuki Kezuka *, Kosuke Kawai, Kenichiro Eguchi and Masahiko Tajika

Shiraishi Central Laboratories Co. Ltd., 4-78 Motohama-cho, Amagasaki, Hyogo 660-0085, Japan; kawai_kosuke@shiraishi.co.jp (K.K.); eguchi_kenichiro@shiraishi.co.jp (K.E.); tajika_masahiko@shiraishi.co.jp (M.T.)

* Correspondence: kezuka_yuki@shiraishi.co.jp; Tel.: +81-6-6417-3130

Received: 24 July 2017; Accepted: 30 July 2017; Published: 1 August 2017

Abstract: Calcium carbonate ($CaCO_3$) occurs in two major polymorphs: rhombohedral calcite and orthorhombic aragonite, the latter is thermodynamically metastable. In this study, we first prepared aragonite needle-like particles by introducing CO_2-containing gas into $Ca(OH)_2$ aqueous slurry. Then, the resulted aragonite particles were heat treated at 500 °C for 1 h, in order to induce the aragonite–calcite phase transition. Particle structures before and after the heat treatment were characterized mainly by powder X-ray diffractometry (XRD), field emission-scanning electron microscopy (FE-SEM) and transmission electron microscopy (TEM). We found that single-crystalline calcite needle-like particles with zigzag surface structures can be fabricated using the phase transition.

Keywords: calcium carbonate; phase transition; calcite; needle-like particle; transmission electron microscopy (TEM)

1. Introduction

In order to design composite materials with desired properties, choosing suitable fillers is crucially important. For instance, mechanical properties of composite materials can be affected by particle morphology and size of fillers [1–5]. In particular, anisotropic materials such as needle-like or fiber-like particles are known to improve mechanical strength of composites much more effectively than spherical particles, because of increase in filler entanglement density. Among a wide variety of fillers, calcium carbonate ($CaCO_3$) is one of the most used fillers in the industry. Calcium carbonate naturally occurs abundantly in the forms of limestone, marble, stalactites, shells, corals, etc. Both ground calcium carbonate (GCC) and precipitated calcium carbonate (PCC) have been used in many industrial fields [6]. The former is obtained by mechanical grinding of limestone and the latter is synthesized mainly using the following reaction:

$$Ca(OH)_2 + CO_2 \rightarrow CaCO_3 + H_2O \quad (1)$$

in recent years, the use of PCC has received much attention, because the particle shape/size of PCCs are relatively uniform and can be controlled by several synthetic conditions [7–10]. For instance, previous studies have shown that dimensional stability and impact strength of plastic composite materials [1–5], mechanical properties of rubber materials [11,12], rheological properties of sealants [13] and gloss characteristics of paper [14,15] can be controlled by changing shape/size of PCCs.

Anhydrous calcium carbonate has three crystalline polymorphs: calcite, aragonite and vaterite. Precipitation in aqueous systems commonly leads to calcite rhombic particles, aragonite needle-like particles and vaterite polycrystalline spherical particles [16–21]. Among the three polymorphs, calcite is the thermodynamically most stable, and vaterite is the least stable [18]. It is reported that metastable aragonite minerals transform into the calcite from 400 to 450 °C, under atmospheric conditions [22,23].

The aragonite–calcite phase transition temperature depends on the origin, crystallinity, calcite content, impurity (e.g., Sr^{2+}) content and water content of aragonite [23–26]. For instance, aragonite phases in biominerals can transform into calcite phases below 350 °C [23]. Here, there are few publications that shed light on the particle morphology changes during the phase transitions. Original morphologies may remain unchanged after the phase transitions.

Synthesis of aragonite needle-like particles, or whiskers, has been studied by many researchers [19–21]. Mg^{2+} ions are known to be one of the most effective impurity ions for the promotion of aragonite formation, because they inhibit the nucleation and crystal growth of calcite [27] and the phase transition from aragonite to calcite [28]. Furthermore, Ota et al. reported that aragonite needle-like particles can be formed efficiently by blowing CO_2-containing gas into $Ca(OH)_2$ suspended $MgCl_2$ aqueous solution [19]. They also mentioned that $MgCl_2$ aqueous solution is reusable for another carbonation process because Mg^{2+} ions and Cl^- ions will not be incorporated into aragonite particles.

In the present study, aragonite needle-like particles were prepared by carbonation reaction of $Ca(OH)_2$ aqueous slurry using CO_2 gas bubbling method, and transformed into the calcite phase by heating at high temperatures. Crystallographic changes and particle morphology changes before and after the heat treatment were investigated mainly by powder X-ray diffractometry (XRD), field emission-scanning electron microscopy (FE-SEM), transmission electron microscopy (TEM) and selected area electron diffraction (SAED) analysis. The main aim of this work is to fabricate and characterize single-crystalline calcite needle-like particles. The fabrication of thermodynamically stable calcite particles with a high aspect ratio may open up new possibilities of PCC as a filling material.

2. Materials and Methods

2.1. Chemicals

To prepare aragonite needle-like particles, chemicals were obtained from manufacturers and used without any purification procedures. $Ca(OH)_2$ aqueous slurry (Taiyo Kagaku Kogyo Kaisha Ltd., Tsukumi, Japan; purity ~99.5%) and $MgCl_2{\cdot}6H_2O$ wafer (Ako Kasei Co., Ltd., Ako, Japan; purity; ~99.8%) were employed as raw materials. CO_2 gas and clean-air was purchased from Showa Denko Gas Products Co., Ltd (Kawasaki, Japan). Impurity content of the starting material, $Ca(OH)_2$, was determined by inductivity coupled plasma-atomic emission spectroscopy (ICP-AES) in an iCE 3300-Uni (Thermo Fisher Scientific Inc., Waltham, MA, USA). Sample preparation for ICP-AES measurement was carried out by the following steps: (1) dissolution of 0.5 g of the powder in 2 mL of nitric acid, (2) dilution up to 100 mL with distilled water, and (3) heating at 180 °C for 1 h.

2.2. Synthetic Procedures and Heat Treatments

Synthetic procedures were determined by following the well-established methods in the literature [19–21]. Aqueous suspension with 1.5 wt % $Ca(OH)_2$ and 4.3 wt % $MgCl_2$ (the molar ratio Ca/Mg = 1/2.3) were prepared by dilution and agitation. The suspension was poured into the reaction tank made of stainless steel and maintained at 70 °C. A CO_2 (30%)-clean air (70%) mixed gas was introduced into the tank from the bottom until pH reached 6.7, at an approximate rate of 900 mL/min for 100 g of $Ca(OH)_2$. During the reaction, the suspension was mechanically stirred at an approximate constant rate of 350 rpm, and pH of the suspension was monitored using a handheld electrical pH meter (DKK-TOA Co., WM-32EP, Tokyo, Japan). After the carbonation, the suspension was dehydrated and dried.

About 5 g of thus prepared powder was put into a crucible and placed in an electric furnace. The powder was then heat treated at 500 °C for 1 h in air, so as to induce the aragonite–calcite phase transition. Then, the sample was slowly furnace-cooled to room temperature.

2.3. Characterization

The as-prepared calcium carbonate dry powder was subjected to the simultaneous thermogravimetry-differential thermal analysis (TG-DTA) (Thermo plus EVO2, Rigaku Co., Ltd., Tokyo, Japan). Here, approximately 20.0 mg powder was placed in a platinum pan and heated at a rate of 20 °C/min up to 1000 °C under the clean-air flow (500 mL/min).

The crystallographic phases were identified by powder XRD (MultiFlex, Rigaku Co. Ltd., Tokyo, Japan) with Cu-K_α line (X-ray wavelength λ = 0.154 nm) at 40 kV and 40 mA. The XRD patterns were collected in the range from 2θ = 20° to 50°, at a counting rate of 2θ = 0.02°/s. The polymorphic ratio (aragonite content ratio) in the powder sample was estimated from the peak intensity ratio, using the following equation:

$$F_a = \frac{(I_{a111} + I_{a221})}{(I_{a111} + I_{a221} + 0.5 \times I_{c104})} \times 100 \quad (2)$$

where F_a is the fraction (wt %) of aragonite and I_{a111}, I_{a221} and I_{c104} are the intensities of the aragonite (111) reflection peak at 26.3°, the aragonite (221) reflection peak at 45.9° and the calcite (104) reflection peak at 29.5°, respectively [20,29].

The particle morphologies were observed by FE-SEM (JSM-6330F, JEOL Co. Ltd., Tokyo, Japan) equipped with a field emission electron gun operated at 3.0 kV and TEM (JEM-2100HR, JEOL Co. Ltd., Tokyo, Japan) equipped with a LaB_6 electron gun operated at 200 kV. Furthermore, SAED patterns were taken in TEM, in order to analyze the crystallographic structure changes. Here, specimens for SEM observations were prepared by mounting powder samples on an electrically conductive tape and coated with gold using a FINE COATER JFC-1200 (JEOL Co. Ltd., Tokyo, Japan) to impart conductivity. Specimens for TEM observations were prepared by dispersing the sample particles into ethanol to the concentration of 0.8 wt %, dropping the suspension on carbon/collodion-coated copper grids, removing excess ethanol and drying.

The Brunauer-Emmett-Teller (BET) one-point method was applied to measure the specific surface area (SSA) of the samples. Measurements were made by nitrogen gas adsorption to the particle surfaces at liquid nitrogen temperature [30,31] using a Macsorb HM Model-1208 (Mountech Co. Ltd., Tokyo, Japan). The powder samples were pre-heated at 110 °C for 1 h in vacuum and degassed at 110 °C for 20 min in vacuum, respectively.

3. Results and Discussion

3.1. Elemental Analysis and Carbonation Reaction

The impurity concentrations of the starting material, $Ca(OH)_2$, determined by the ICP-AES technique are listed in Table 1. Figure 1 shows the pH change in the slurry as the function of carbonation reaction time. The neutralization reaction seems to be completed within 350 min under the present experimental system. Ota et al. pointed out that keeping the pH value of the slurry < 9 during the carbonation reaction was important for efficient formation of aragonite particles [19]. The present system fulfilled that criteria; thus, aragonite particles should be favorably produced. This will be confirmed later. Gas efficiency can be estimated by comparing the total volume of CO_2 introduced to the slurry and the amount of resulted calcium carbonate particles. Assuming the completion of the neutralization reaction at 6.7 in pH, which correspond to the reaction time of 350 min, the gas efficiency was roughly estimated to be 32%.

Table 1. Impurity concentrations, in μg/g (ppm), in the $Ca(OH)_2$ used in this study measured by ICP-AES.

Mg	Sr	Si	P	Fe	Na	Al	Mn
2900	360	450	55	96	65	190	10

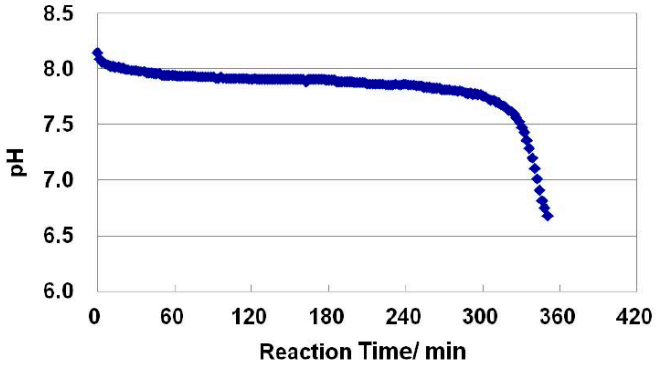

Figure 1. The change in pH of the slurry during the carbonation of $Ca(OH)_2$ at 70 °C with the approximate flow rate of 900 mL/min of CO_2 (30%)-clean air (70%) mixed gas for 100 g of $Ca(OH)_2$, as the function of reaction time.

3.2. Thermal Analysis

Figure 2 shows simultaneously taken TG-DTA curves of the as-prepared calcium carbonate dry powder synthesized in this study. An initial weight loss of 0.5 wt % until the temperature reaches 372 °C is mainly attributed to desorption of water and organic species physically absorbed on the particle surface. Then, a small endothermic peak between 372 °C and 436 °C, accompanied with a weight loss of 0.8%, can be confirmed. This is considered to be the sum of the removal of water from residual $Ca(OH)_2$, according to the following equation:

$$Ca(OH)_2 \rightarrow CaO + H_2O \quad (3)$$

and the aragonite–calcite phase transition. Phase transition temperature from aragonite to calcite varies with states of aragonite; mineral origin aragonite tends to transform at higher temperatures (<450 °C) compared to aragonitic biominerals such as shells and coral (<350 °C) [23]. Thereafter, a larger endothermic peak between 552 °C and 806 °C, accompanied with the main weight loss of 42.4%, can be seen. This is assigned to the elimination of carbon dioxide along with the carbonate decomposition according to the following equation:

$$CaCO_3 \rightarrow CaO + CO_2 \quad (4)$$

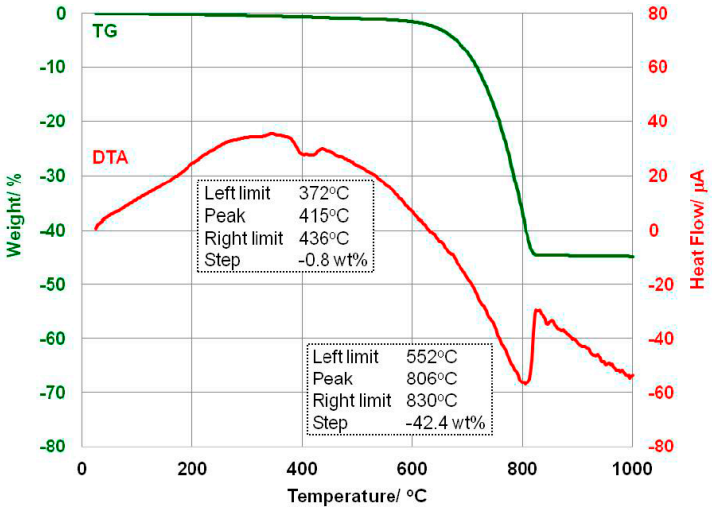

Figure 2. Simultaneous TG (green)-DTA (red) curves of the as-prepared calcium carbonate powder.

Further decrease in the sample weight is negligible until the temperature reaches 1000 °C. The heat treatment temperature chosen in this study, 500 °C, is located in the middle of the two endothermic peaks so that it can be anticipated that the phase transition would occur, but the decarbonation will not occur during the heat treatment.

3.3. Identification of Crystallographic Phases

Figure 3 shows the XRD patterns of the powders before (blue) and after (red) the heat treatment at 500 °C for 1 h. The major peaks for aragonite and calcite, used in Equation (2), are explicitly indicated in the figure. For the XRD pattern of the powder before the heat treatment (blue), all of the peaks were indexed as either orthorhombic aragonite phase or rhombohedral calcite phase. According to Equation (2), the aragonite content in the as-prepared powder was calculated approximately to be 96 wt %. The presence of unreacted $Ca(OH)_2$ was not detected within the sensitivity of the XRD analysis. This indicates that only a trace amount of $Ca(OH)_2$ remained in the powder, if any. On the other hand, for the XRD pattern of the powder after the heat treatment (red), the presence of aragonite phase is not confirmed. This indicates that all the aragonite particles transformed into calcite phase due to the heat treatment. The Scherer equation [32] was not applicable to calculate the crystallite sizes of the aragonite and calcite particles from the XRD patterns, because the peaks were highly sharp and not enough peak broadenings were observed. This suggests that both particles were greater than 100 nm.

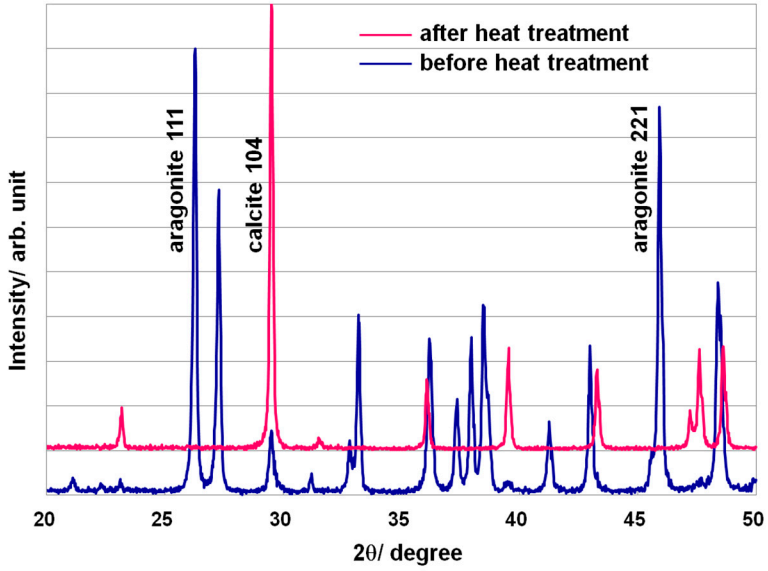

Figure 3. Powder XRD patterns of the calcium carbonate particles before (blue) and after (pink) the heat treatment.

3.4. Particle Characterization

Figure 4 shows low- and high-magnification SEM images for aragonite powder (Figure 4a,c) and for calcite powder (Figure 4b,d). It is clear that the carbonation reaction produced aragonite needle-like particles. These particles have sizes of 3–10 μm in length and 130–280 nm in width, i.e., the aspect ratio ranged from 10 to 30. On the other hand, it was confirmed that the calcite particles almost preserved the needle-like morphology of the aragonite particles. Therefore, it is concluded that the calcite needle-like particles are successfully fabricated via the phase transition of aragonite due to heating at 500 °C for 1 h. Here, it can be seen in Figure 4d that calcite needle-like particles have rougher surfaces compared to aragonite needle-like particles. In addition, some of the calcite needle-like particles are slightly winding. This might indicate that the particle morphology changes has not thoroughly completed for all the particles by the heat treatment conditions employed in this study, even after the aragonite–calcite

phase transition has completed. The densities of aragonite and calcite are 2.93 g/mm^3 and 2.71 g/mm^3, respectively. Therefore, volume expansion of about 8%, which corresponds to the length and width expansion of about 2%, should occur after the phase transition, whereas, these are not confirmed by the SEM observations in this study, because powder samples were directly observed and most of the needle-like particles in the images are being inclined.

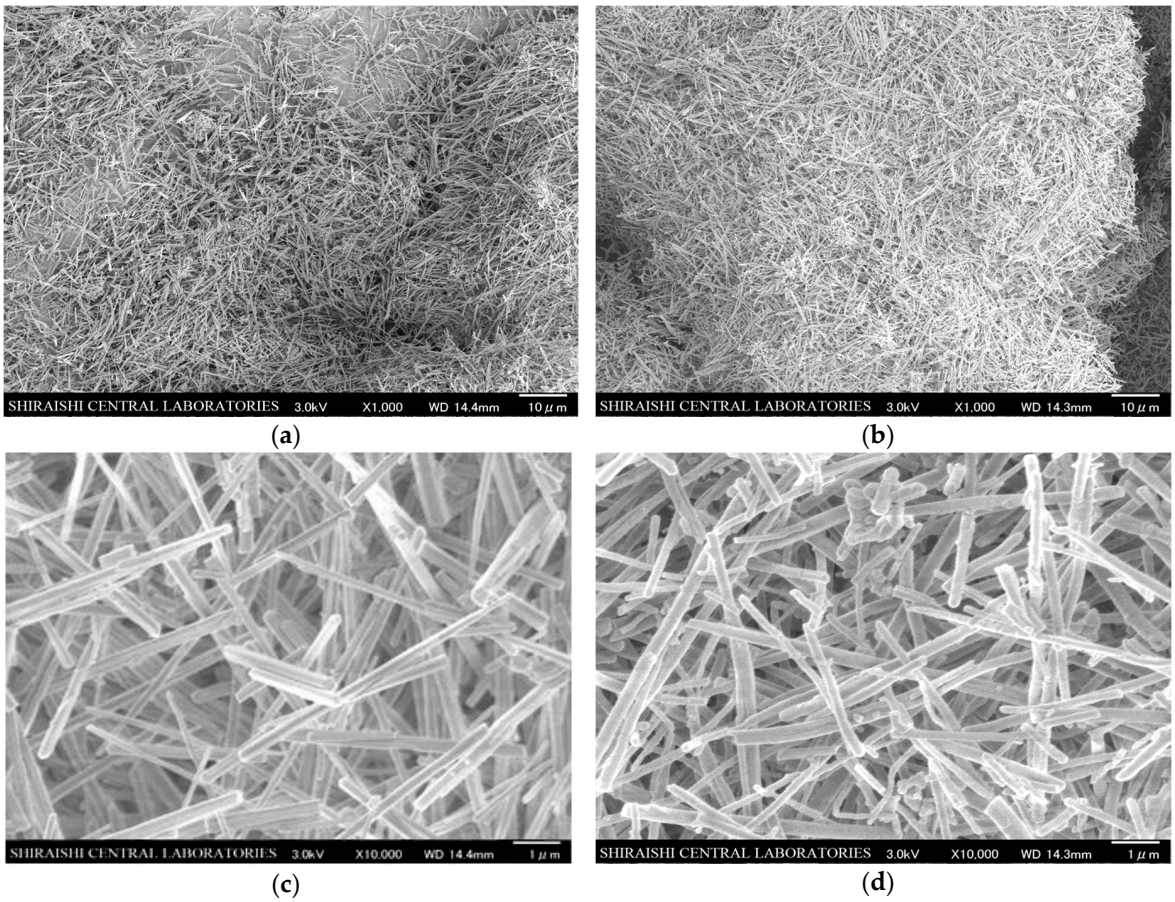

Figure 4. Low- and high-magnification SEM images for aragonite powder (**a**,**c**) and for calcite powder (**b**,**d**). Scale-bars are 10 μm for low-magnification and 1 μm for high-magnification observations. The needle-like morphology of aragonite particles was maintained even after the heat treatment, to form calcite needle-like particles.

BET-SSA of the aragonite needle-like particles and the calcite needle-like particles are measured to be 6.6 m^2/g and 6.0 m^2/g, respectively. These small values might indicate that both particles are solid crystals without pores.

In order to clarify the particle structures in more detail, TEM observations were carried out for both samples. Figure 5a shows a bright-field TEM image of an aragonite particle. The insert is a SAED pattern taken along the [1$\bar{1}$0] axis of the aragonite structure. A single-crystalline aragonite needle-like particle is observed. The long axis of the aragonite particle is along the *c*-axis, as reported in the literature [19]. Figure 5b shows a bright-field TEM image of a calcite particle after the heat treatment. A needle-like particle with zigzag surface structure is observed. Judging only from the TEM image, the particle looks superficially polycrystalline. Each surface step is parallel to one another, and the length between each surface steps is approximately 10–40 nm. The insert is a SAED pattern taken along the [241] axis of the calcite structure. Here, splitting of the diffraction spots is not observed in the SAED pattern. This means that the crystallographic orientation differences between neighboring nano-blocks are negligibly small and each calcite needle-like particle is almost single-crystalline.

Thus, it is deduced that the darker contrasts in between the neighboring nano-blocks are caused by the surface steps. It is concluded that a fabrication method of single-crystalline calcite particles with a high aspect ratio using the aragonite–calcite phase transition is established. The use of the calcite needle-like particles as fillers may be beneficial for strengthening composites, because the filler-matrix contacting area per filler length becomes larger by the zigzag surface structures.

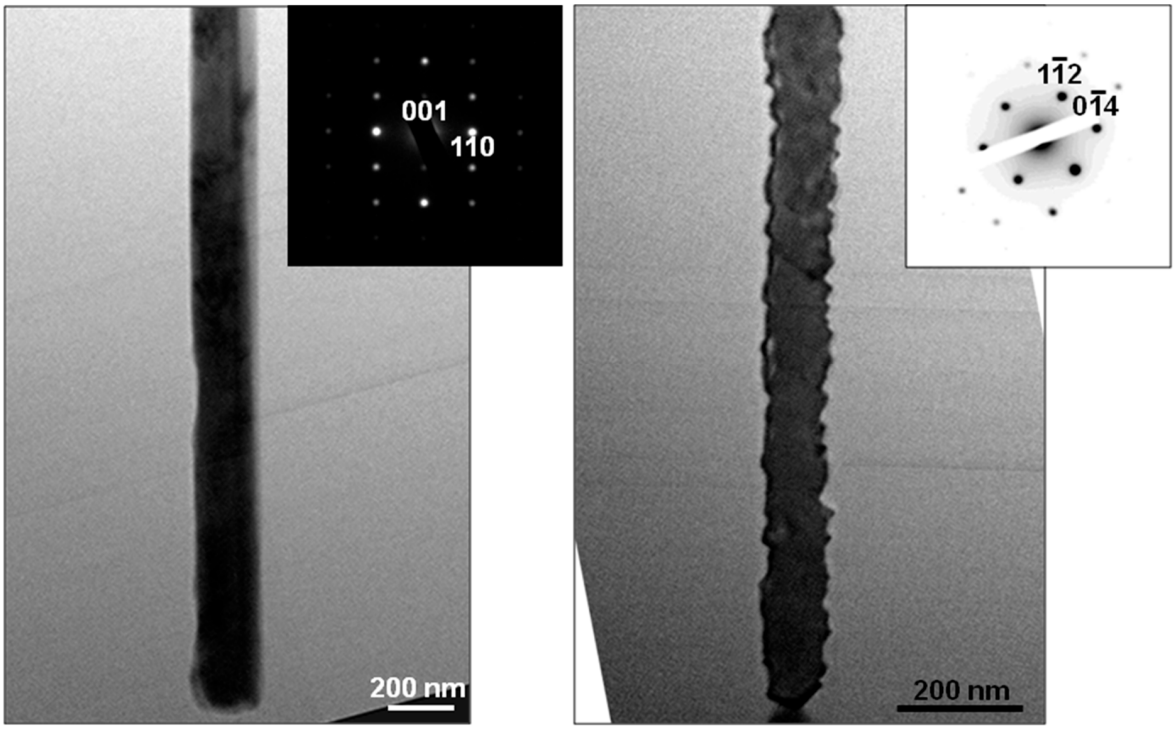

Figure 5. Bright-field TEM images of (**a**) an aragonite needle-like particle and (**b**) a calcite needle-like particle with corresponding SAED patterns. SAED patterns indicate that both particles are single-crystalline.

4. Conclusions

Aragonite needle-like particles were synthesized by bubbling CO_2-containing gas into $Ca(OH)_2$ aqueous slurry with the presence of enough amount of $MgCl_2$. It was elucidated that calcite needle-like particles can be fabricated by calcining aragonite needle-like particles at 500 °C for 1 h in air. By TEM observations, it was found that the fabricated calcite needle-like particles have zigzag surface structures. SAED analyses revealed that neighboring nano-blocks are highly mono-oriented to one another to form almost single-crystalline particles. This fabrication method of thermodynamically stable calcite needle-like particles may broaden the applications of calcium carbonate as a filling material.

Acknowledgments: We thank Akiyoshi Osaka, Yuichi Ikuhara, Eita Tochigi, and two anonymous reviewers for useful discussion and thoughtful comments.

Author Contributions: Yuki Kezuka, Kosuke Kawai, Kenichiro Eguchi, and Masahiko Tajika conceived and designed the experiments; Yuki Kezuka, Kosuke Kawai, and Kenichiro Eguchi performed the experiments, analyzed the data, and contributed reagents/materials/analysis tools; Yuki Kezuka wrote the paper.

Conflicts of Interest: The authors declare no conflicts of interest.

References

1. Eirich, F.R. *Handbook of Fillers and Reinforcements for Plastics*; Katz, H.S., Milewski, J.V., Eds.; Litton Educational Publishing, Inc.: New York, NY, USA, 1978.

2. Bartczak, Z.; Argon, A.S.; Cohen, R.E.; Weinberg, M. Toughness mechanism in semi-crystalline polymer blends: II. High-density polyethylene toughened with calcium carbonate filler particles. *Polymer* **1999**, *40*, 2347–2365. [CrossRef]
3. Da Silva, A.L.N.; Rocha, M.C.G.; Moraes, M.A.R.; Valente, C.A.R.; Coutinho, F.M.B. Mechanical and rheological properties of composites based on polyolefin and mineral additives. *Polym. Test.* **2002**, *21*, 57–60. [CrossRef]
4. Thio, Y.S.; Argon, A.S.; Cohen, R.E.; Weinberg, M. Toughening of isotactic polypropylene with $CaCO_3$ particles. *Polymer* **2002**, *43*, 3661–3674. [CrossRef]
5. Lama, T.D.; Hoang, T.V.; Quang, D.T.; Kim, J.S. Effect of nanosized and surface-modified precipitated calcium carbonate on properties of CaCO3/polypropylene nanocomposites. *Mater. Sci. Eng. A* **2009**, *501*, 87–93. [CrossRef]
6. Roskill Information Services Ltd. *Ground and Precipitated Calcium Carbonate: Global Industry Markets and Outlook*, 1st ed.; Roskill Information Services Ltd.: London, UK, 2012; pp. 270–359.
7. Shiraishi, T. Colloidal Calcium Carbonate and Method of Producing the Same. U.S. Patent No. 1,654,099, 27 December 1927.
8. Shiraishi, T. Method of Manufacturing Colloidal Carbonate of Alkali Earths. U.S. Patent No. 1,863,945, 21 June 1932.
9. Wray, J.L.; Daniels, F. Precipitation of Calcite and Aragonite. *J. Am. Chem. Soc.* **1957**, *79*, 2031–2034. [CrossRef]
10. Yamada, H.; Hara, N. Formation Process of Colloidal Calcium Carbonate in the Reaction of the System $Ca(OH)_2$-H_2O-CO_2. *Gypsum Lime* **1985**, *194*, 3–12.
11. Payne, A.R. Dynamic Properties of Filler-Loaded Rubbers. In *Reinforcement of Elastomers*; Kraus, G., Ed.; John Wiley & Sons, Inc.: New York, NY, USA, 1965; pp. 69–124.
12. Fang, Q.; Song, B.; Tee, T.; Sin, L.T.; Hui, D.; Bee, S. Investigation of dynamic characteristics of nano-size calcium carbonate added in natural rubber vulcanizate. *Compos. Part B* **2014**, *60*, 561–567. [CrossRef]
13. Damusis, A. Pigments in Sealants. In *Sealants*; Damusis, A., Ed.; Reinhold Publishing Co.: New York, NY, USA, 1967; pp. 52–91.
14. Hagemeyer, R.W. *Pigments for Paper*, 1st ed.; O'Shea, J.E., Ed.; Tappi Press: Atlanta, GA, USA, 1997.
15. Kumar, N.; Bhardwaj, N.K.; Chakrabarti, S.K. Influence of pigment blends of different shapes and size distributions on coated paper properties. *J. Coat. Technol. Res.* **2011**, *8*, 605–611. [CrossRef]
16. García-Carmona, J.; Morales, J.G.; Clemente, R.R. Morphological control of precipitated calcite obtained by adjusting the electrical conductivity in the $Ca(OH)_2$–H_2O–CO_2 system. *J. Cryst. Growth* **2003**, *249*, 561–571. [CrossRef]
17. Han, Y.S.; Hadiko, G.; Fuji, M.; Takahashi, M. Factors affecting the phase and morphology of $CaCO_3$ prepared by a bubbling method. *J. Eur. Ceram. Soc.* **2006**, *26*, 843–847. [CrossRef]
18. Somani, R.S.; Patel, K.S.; Mehta, A.R.; Jasra, R.V. Examination of the Polymorphs and Particle Size of Calcium Carbonate Precipitated Using Still Effluent (i.e., $CaCl_2$ + NaCl Solution) of Soda Ash Manufacturing Process. *Ind. Eng. Chem. Res.* **2006**, *45*, 5223–5230. [CrossRef]
19. Ota, Y.; Inui, S.; Iwashita, T.; Kasuga, T.; Abe, Y. Preparation of Aragonite whiskers. *J. Am. Ceram. Soc.* **1995**, *78*, 1983–1984. [CrossRef]
20. Park, W.K.; Ko, S.J.; Lee, S.W.; Cho, K.H.; Ahn, J.W.; Han, C. Effects of magnesium chloride and organic additives on the synthesis of aragonite precipitated calcium carbonate. *J. Cryst. Growth* **2008**, *310*, 2593–2601. [CrossRef]
21. Hu, Z.; Shao, M.; Cai, Q.; Ding, S.; Zhong, C.; Wei, X.; Deng, Y. Synthesis of needle-like aragonite from limestone in the presence of magnesium chloride. *J. Mater. Process. Technol.* **2009**, *209*, 1607–1611. [CrossRef]
22. Faust, G.T. Differentiation of Aragonite from Calcite by Differential Thermal Analysis. *Science* **1949**, *110*, 402–403. [CrossRef] [PubMed]
23. Omari, H. Thermal stability of calcium carbonate gallstone crystal. *J. Jpn. Biliary Assoc.* **1989**, *3*, 109–117.
24. Rao, M.S.; Yoganarasimhan, S.R. Preparation of pure aragonite and its transformation to calcite. *Am. Mineral.* **1965**, *50*, 1489–1493.
25. Rao, G.V.S.; Natarajan, M.; Rao, C.N.R. Effect of Impurities on the Phase Transformations and Decomposition of $CaCO_3$. *J. Am. Ceram. Soc.* **1968**, *51*, 179–181. [CrossRef]
26. Yoshioka, S.; Kitano, Y. Transformation of aragonite to calcite through heating. *Geochem. J.* **1985**, *19*, 245–249. [CrossRef]

27. Beruto, D.; Giordani, M. Calcite and aragonite formation from aqueous calcium hydrogencarbonate solutions: Effect of induced electromagnetic field on the activity of $CaCO_3$ Nuclei Precursors. *J. Chem. Soc. Faraday Trans.* **1993**, *89*, 2457–24666. [CrossRef]
28. Bischoff, J.L.; Fyfe, W.S. Catalysis, inhibition, and the calcite-aragonite problem; Part 1, The aragonite–calcite transformation. *Am. J. Sci.* **1968**, *266*, 65–79. [CrossRef]
29. Wada, N.; Okazaki, M.; Tachikawa, S. Effects of calcium-binding polysaccharides from calcareous algae on calcium carbonate polymorphs under conditions of double diffusion. *J. Cryst. Growth* **1993**, *132*, 115–121. [CrossRef]
30. Brunauer, S.; Emmett, P.H.; Teller, E. Adsorption of gases in multimolecular layers. *J. Am. Chem. Soc.* **1938**, *60*, 309–319. [CrossRef]
31. Mikhail, R.S.; Brunauer, S. Surface area measurements by nitrogen and argon adsorption. *J. Colloid Interface Sci.* **1975**, *52*, 572–577. [CrossRef]
32. Scherrer, P. Estimation of the size and internal structure of colloidal particles by means of röntgen. *Nachr. Ges. Wiss. Göttingen* **1918**, *2*, 96–100.